AGU PUBLICATIONS

Geophysical Research Letters

RESEARCH LETTER
10.1002/2015GL065813

Key Points:
- Significant convectively coupled MRG waves are disclosed from TRMM-KWAJEX field campaign data
- Composite structures of dynamic and thermodynamic fields of MRG waves are presented
- The coupling between wave dynamics and diabatic heating is explored

Correspondence to:
M. Zhang,
zhang@stonybrook.edu

Citation:
Wang, X., and M. Zhang (2015), The coupling of mixed Rossby-gravity waves with diabatic heating during the TRMM-KWAJEX field campaign, *Geophys. Res. Lett.*, *42*, 8241–8249, doi:10.1002/2015GL065813.

Received 18 AUG 2015
Accepted 15 SEP 2015
Accepted article online 9 OCT 2015
Published online 14 OCT 2015

The coupling of mixed Rossby-gravity waves with diabatic heating during the TRMM-KWAJEX field campaign

Xiaocong Wang[1] and Minghua Zhang[2]

[1]State Key Laboratory of Numerical Modeling for Atmospheric Sciences and Geophysical Fluid Dynamics, Institute of Atmospheric Physics, Chinese Academy of Sciences, Beijing, China, [2]School of Marine and Atmospheric Sciences, Stony Brook University, Stony Brook, New York, USA

Abstract Composite dynamic and thermodynamic structures of mixed Rossby-gravity (MRG) waves are presented with their coupling with diabatic heating and moisture sources/sinks, using Tropical Rainfall Measuring Mission-Kwajalein Experiment (TRMM-KWAJEX) field campaign data. A significant departure of convectively coupled waves from dry waves exists in the phases of wave component: maximum low-level wind convergence is accompanied by midtropospheric divergence and upper tropospheric convergence that is preceded by increase of moisture in the boundary layer. These phases correspond to surface turbulent transport, shallow and midlevel convections that cause moistening and heating of the lower and middle troposphere. They are followed by deep convection with maximum heating centered in the upper troposphere. The deep convective heating evolves to stratiform-like upper tropospheric heating and lower tropospheric cooling that precedes the quick demise of convection. Such a structure on convectively coupled MRG waves is summarized by four phases, which sheds lights on how tropical waves are coupled with convective processes in all their phases.

1. Introduction

Convectively coupled equatorial waves are important in tropical weather and climate. They span a wide range of spatial and temporal scales [*Wheeler and Kiladis*, 1999]. Diabatic heating plays a key role in the excitation and maintenance of these waves. It supplies the energy from the surface to offset the radiative and frictional damping of tropical waves.

Understanding the coupling between the wave dynamics and the associated diabatic heating fields has been a subject of research in the last 50 years [e.g., *Lindzen*, 1974; *Neelin and Held*, 1987; *Zhang and Geller*, 1994; *Zhang*, 2005]. Much has been learned in the last 30 years about the structure of these waves from observational composite analyses [e.g., *Liebmann and Hendon*, 1990; *Takayabu and Nitta,* 1993*; Takayabu et al.,* 1996*; Wheeler and Kiladis,* 1999*; Kikuchi and Takayabu,* 2004*; Tai and Ogura,* 1987*; Yokoyama and Takayabu,* 2012] and about the role of diabatic heating in these waves [*Mapes et al.,* 2006*; Khouider and Majda,* 2008*; Kuang*, 2008]. Correctly simulating these waves, however, remains a significant challenge in the modeling community [*Lin et al.,* 2006].

To understand how wave dynamics drives the heating field and how heating drives the dynamics, detailed time-space distribution of the heating field and its association with the wave dynamics are needed. Observational data of such information however are generally lacking. The purpose of this paper is to present the coupled structure of wave dynamics and diabatic heating by using the constrained variational objective analysis of the coordinated 6-hourly balloon sounding data and surface measurements during the NASA Tropical Rainfall Measuring Mission (TRMM) Kwajalein Experiment (KWAJEX). Along with the dynamic and thermodynamic structures of the waves, we present the evolution of the heating fields associated with planetary boundary layer (PBL) turbulence, shallow and deep convections in different phases of the waves.

2. Data and Methodology

KWAJEX was conducted around the Kwajalein Atoll in the Republic of the Marshall Islands (7–10°N, 166–169°E) for 53 days from 24 July 1999 to 15 September 1999. It used data from six coordinated balloon sounding stations with 6-hourly upper air measurements of winds, temperature and humidity, which are augmented

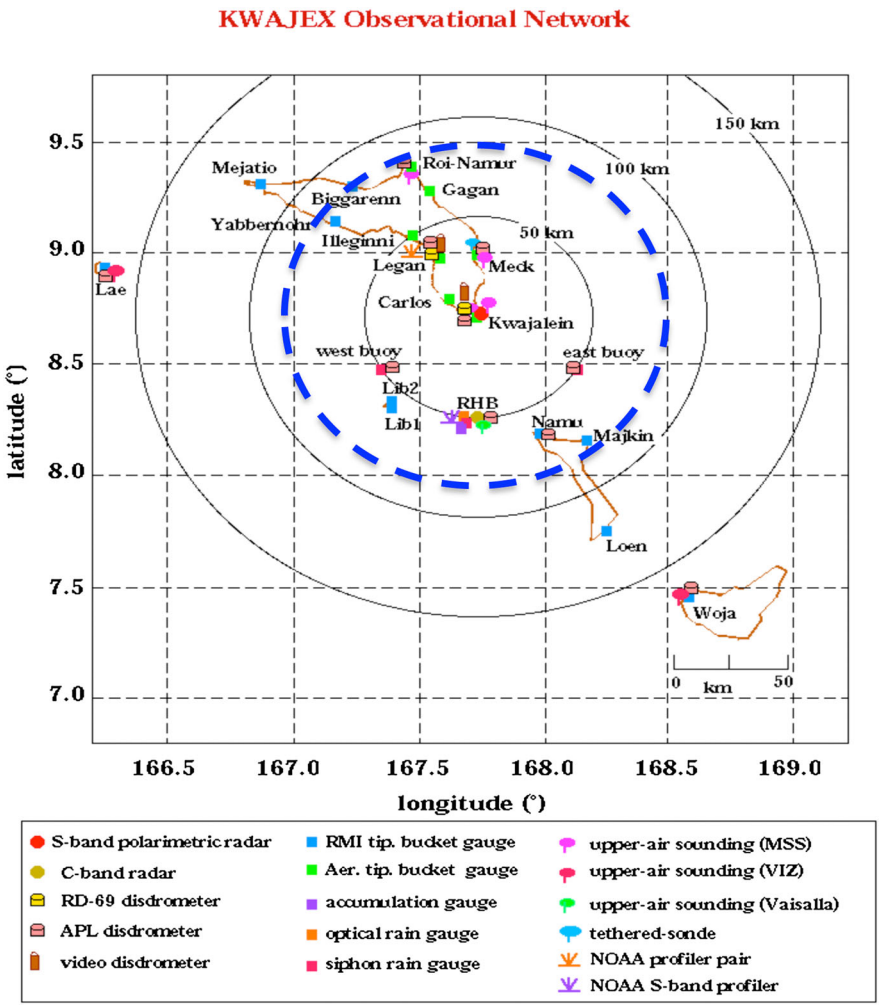

Figure 1. Locations of surface and upper air measurement stations during TRMM KWAJEX. The blue dashed circle is the domain of the variational objective analysis of diabatic heating and other atmospheric fields.

by three nearby operational sounding stations with 12-hourly data; an S-Pol radar; two buoys; and a number of surface meteorological measurements from several island stations within the radius of about 150 km centered at Kwajalein (8.6°N, 167.4°E). The distribution of the measurement stations is shown in Figure 1. Several studies have analyzed the meteorology, clouds, precipitation by using the aircraft, upper air sounding sites, ships and a collection of remote and in situ surface-based sensors [*Sobel et al.,* 2004; *Yuter et al.,* 2005; *Schumacher et al.,* 2007, 2008].

The variational objective analysis of the diabatic heating is conducted following the methods of *Zhang and Lin* [1997] and *Zhang et al.* [2001]: First, all upper air and surface measurements are subject to rigorous quality control and preprocessing, which are described in *Zhang et al.* [2001]. Upper air measurements include the 6-hourly balloon sounding data from the six KWAJEX stations and 12-hourly sounding data from three nearby operational weather stations. Surface rain data were from the gridded S-Pol radar retrievals and surface gauge measurements [*Schumacher and Houze,* 2000]. Precipitation is averaged over the domain that corresponds to the analysis of the upper air vertical velocity and other derived fields denoted by the dashed blue circle in Figure 1. The radar and gauge precipitation data sets are equally averaged to give an estimate of the domain-averaged precipitation. The collocated radiative fluxes at the top-of-the atmosphere (TOA) and surface are from the International Satellite Cloud Climatology Project [*Zhang et al.,* 1995]. Due to the lack of sufficient sampling, surface sensible and latent heat fluxes are from the National Centers for Environmental Prediction/National Center for Atmospheric Research (NCEP/NCAR) reanalysis [*Kistler et al.,* 2001].

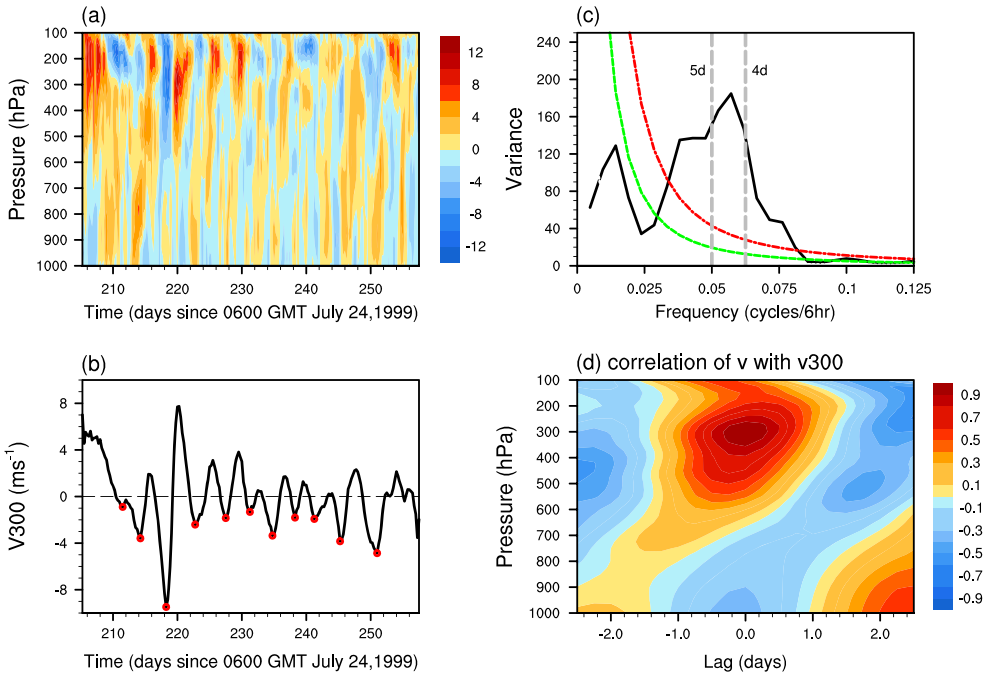

Figure 2. (a) Meridional wind from the variational analysis during KWAJEX from 24 July 1999 to 15 September 1999 (unit: m/s). (b) Meridional wind at 300 hPa after the removal of time average and diurnal cycle (unit: m/s). (c) Power spectrum of the 300 hPa meridional wind (unit: m^2/s^2). The red and green curves, respectively, denote "Red Noise" spectrum and 95% confidence for Markov. (d) Lag correlation of meridional winds with 300 hPa meridional wind.

In the second step, the 6-hourly NCEP/NCAR reanalysis during the KWAJEX period is used as a background atmospheric state. The background winds, temperature, and water vapor mixing ratio are then variationally adjusted by minimizing a cost function relative to the quality-controlled sounding data with constraints that the final analysis satisfies the column-integrated conservation of air mass, energy, water, and momentum in any 6 h time interval during KWAJEX in the analysis domain of Figure 1.

Finally, the line integral method is used to calculate the horizontal fluxes into or out of the analysis domain. Vertical velocity and advective tendencies are derived from the flux calculations. The 6-hourly diabatic heating field ($Q1$) and moisture sink ($Q2$) [*Yanai et al.,* 1973] are derived as residuals of the thermodynamic equation and the water vapor mass continuity equation. The use of the surface and TOA data for the analysis is a unique feature of the approach that improves the quality of the diabatic heating field. While uncertainties of the analyzed data have not been quantified, they are the best available estimate.

This variationally analyzed product has been used in *Schumacher et al.* [2008] to describe the heating profiles associated with different cloud types and in *Zhang and Hagos* [2009] to investigate the different modes of diabatic heating. The analyzed vertical velocities and advective tendencies have been also used to force cloud-resolving models or single-column models [e.g., *Blossey et al.*, 2007; *Zeng et al.*, 2008; *Li et al.*, 2008; *Wang and Zhang*, 2013].

3. Results

3.1. Wave Structure

Figure 2a displays the time-pressure cross section of the meridional wind. During the entire period, the southerly and northerly winds alternate with time every 3 to 6 days. The periodic behavior can be more clearly seen in the time series of the meridional wind at 300 hPa ($V300$, hereafter) shown in Figure 2b. In this figure, the diurnal and time-averaged components are removed. The power spectrum of $V300$ indicates statistically significant power centered at the period of about 4.5 days (Figure 2c). This period is consistent with mixed Rossby-gravity (MRG) waves in the equatorial Pacific that has been previously reported [e.g., *Straub and Kiladis,* 2003; *Aiyyer and Molinari*, 2003; *Swann et al.,* 2006; *Liebmann and Hendon*, 1990; *Takayabu and Nitta*, 1993].

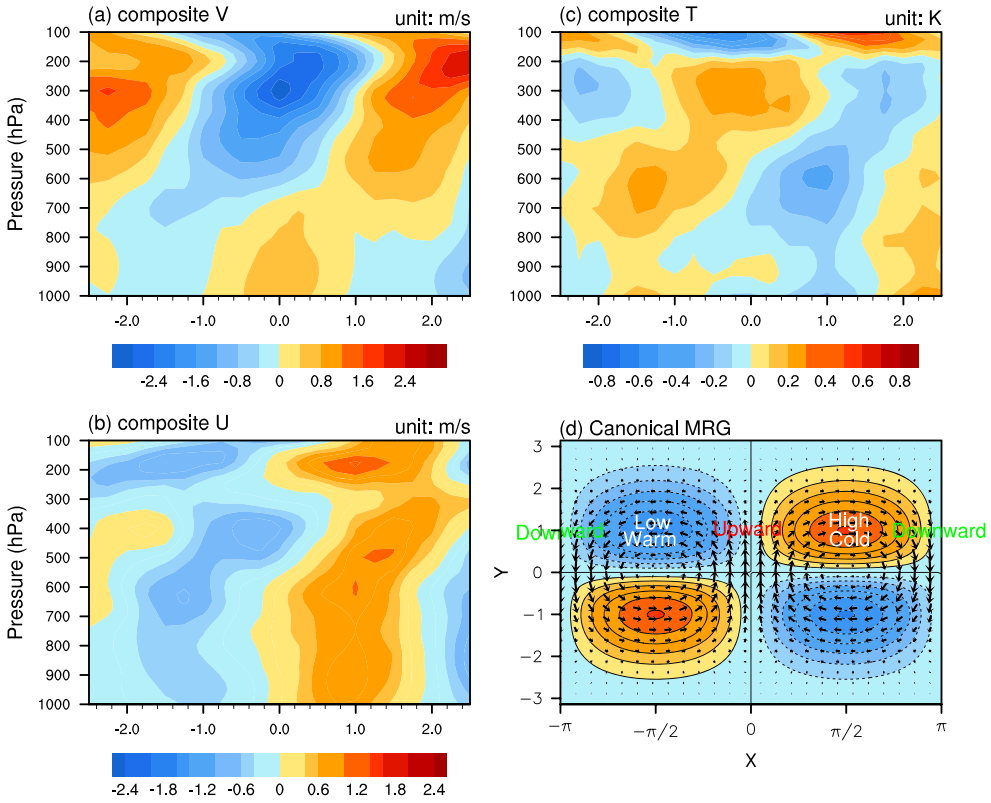

Figure 3. Composite of anomalies of (a) meridional wind based on the minimum 300 hPa meridional wind (unit: m/s), (b) zonal wind (unit: m/s), and (c) temperature (unit: K). (d) Horizontal structure of the canonical MRG wave in the lower troposphere. The phases of geopotential height, temperature, and vertical velocity are labeled. Color represents pressure field. The magnitudes are only schematic.

Figure 2d shows the lag correlation of the meridional wind against *V*300. It can be seen that at other levels it is coherently correlated; wind directions in the upper and low levels are opposite to each other. There is a backward tilt of the wave with height, which is commonly observed in other convectively coupled waves [e.g., *Takayabu et al*., 1996; *Straub and Kiladis*, 2003]. The wave period is about 4.5 days, consistent with the power spectrum analysis.

In Figures 3a–3c, we show the composite structure of the meridional and zonal winds and temperature. In this figure, day 0 corresponds to the time of minima at 300 hPa, which are marked in red in Figure 2b. The structure of the composite meridional wind is similar to the lag correlation in Figure 2d. It is similar to the canonical MRG wave in the dry atmosphere with opposite signs of winds in the upper and lower troposphere. In Figure 3d, we give the horizontal structure of a canonical MRG wave in the lower troposphere as a reference where the maximum phase of winds, geopotential height, temperature, and vertical velocity are marked.

In the observational composite of Figures 3a–3c, in the lower troposphere below about 500 hPa, the phase relationships of the zonal wind and temperature with the meridional wind in the composite waves are the same as those in the canonical MRG wave: Zonal wind lags meridional wind by a quarter cycle, and temperature leads the meridional wind by a quarter cycle. In these waves, wind acceleration in the zonal direction is driven by the Coriolis force from the meridional wind that dominates over the zonal pressure gradient force, while the meridional wind acceleration is driven by the Coriolis force from the zonal wind. These momentum forces drive the wave propagating westward. In the canonical MRG wave, the vertical velocity is determined by the meridional wind convergence in the lower troposphere that dominates over the zonal wind divergence. The upward motion cools the atmosphere, leading to the westward propagation of the cold phase of the MRG wave. The cold phase therefore lags the low-level meridional wind by a quarter cycle. These features are all present in the observational composite of the waves in the lower troposphere. We therefore identified the composite wave as the MRG wave.

Above 500 hPa, however, unlike the canonical MRG wave in a dry atmosphere, temperature field in the convectively coupled wave is shifted eastward, with the warm phase almost in sync with the low-level meridional wind. We further point out that while the temperature field exhibits an eastward tilt with height, the phase transition is not smooth. A sharp phase transition is seen at around 500 hPa. This transition will be shown as coincident with the transition between shallow convection to deep convection. Another feature of the wave structure that differs from the canonical MRG is that the zonal wind around 200 hPa is almost in phase with the zonal wind in the lower troposphere. This difference may be related with the redistribution of the pressure gradient force that is associated with the temperature phase shift.

3.2. Coupling With Diabatic Heating

To reveal the unique coupling of the MRG wave with diabatic heating, we show in Figure 4a the composite of the horizontal divergence of winds. In the lower troposphere below 700 hPa, the divergence field is in opposite phase to the meridional wind, which is the same as for the canonical MRG wave. Above 700 hPa, however, there is a maximum wind divergence in the middle of the troposphere from 700 hPa to 400 hPa at the time of maximum low-level wind convergence, and there is wind convergence near 200 hPa at the same time. As a result, in the positive phase of the low-level meridional wind, the vertical velocity is upward in the lower troposphere but downward in the upper troposphere as shown in Figure 4b. This vertical distribution of the wind convergence field confirms results from previous composite analyses using band-passed global data [e.g., *Tai and Ogura*, 1987; *Yokoyama and Takayabu,* 2012].

This structure of wave number 1 in height in the vertical velocity is associated with shallow convection and cumulus congestus. This can be seen in the apparent heating $Q1$ (Figure 4d), which is limited below 500 hPa during the phase of maximum surface wind convergence. The lower tropospheric heating associated with the low-level southerly is in agreement with the conventional thinking that the low-level convergence leads to upward motion which then causes diabatic heating. Why is then low-level convergence not associated with upward motion in the upper troposphere?

The relationship between the moisture field (Figure 4c) and the $Q1$ (Figure 4d) gives hint of an explanation. The humidity field shows an eastward tilt with height, with three maxima near the surface, between 600 and 700 hPa and between 400 and 500 hPa. During the initial phase of the low-level wind convergence, the upper troposphere is still dry, and only shallow convection/cumulus congestus is active. After the shallow convection moistens the middle troposphere in the later phase of the low-level convergence, deep convection then occurs. Deep convection significantly warms the upper troposphere with a single mode of low-level convergence and strong upper level divergence.

A comparison of the $Q1$ (Figure 4d) and $Q2$ (Figure 4e) fields reveals additional details of the coupling of these diabatic fields with the dynamics. In the early phase of the low-level convergence (around -0.9 to -0.7 days), Q1 is positive between 700 and 800 hPa, but $Q2$ is initially negative. This opposite sign implies sources of both heat and moisture that can only be explained by vertical turbulent transport of heat and moisture through PBL or nonprecipitating shallow convection instead of condensational heating. This can be confirmed in the $Q_1 - Q_2 - Q_{\mathrm{rad}}$ field that represents the vertical subgrid-scale transport of moist static energy shown in Figure 4f:

$$Q_1 - Q_2 - Q_{\mathrm{rad}} = -\overline{\frac{\partial \omega' h'}{\partial p}} \tag{1}$$

where the radiative heating rate Q_{rad} is calculated from Cloud-Resolving Model by using the System of Atmospheric Models [*Khairoutdinov and Randall,* 2003], ω' and h' are deviations of the pressure vertical velocity and moist static energy from the domain averages. Figure 4f shows that before the low-level convergence, there is accumulation of moist static energy in the PBL through the subgrid-scale transport. In the initial phase of the low-level convergence, the positive $-\overline{\frac{\partial \omega' h'}{\partial p}}$ rises with negative values near the surface. This is an indication of vertical heat transport by shallow convection. In the later phase of the low-level convergence, the $-\overline{\frac{\partial \omega' h'}{\partial p}}$ shows a deep layer of negative tendency below 600 hPa and positive tendency above 600 hPa. This is a signature of deep convection with maximum convective vertical transport of moist static energy at 600 hPa. In addition to the vertical subgrid-scale transport, in the later phase of lower tropospheric convergence, $Q1$ and $Q2$ are both positive, suggesting condensational heating in both shallow convection and deep convection.

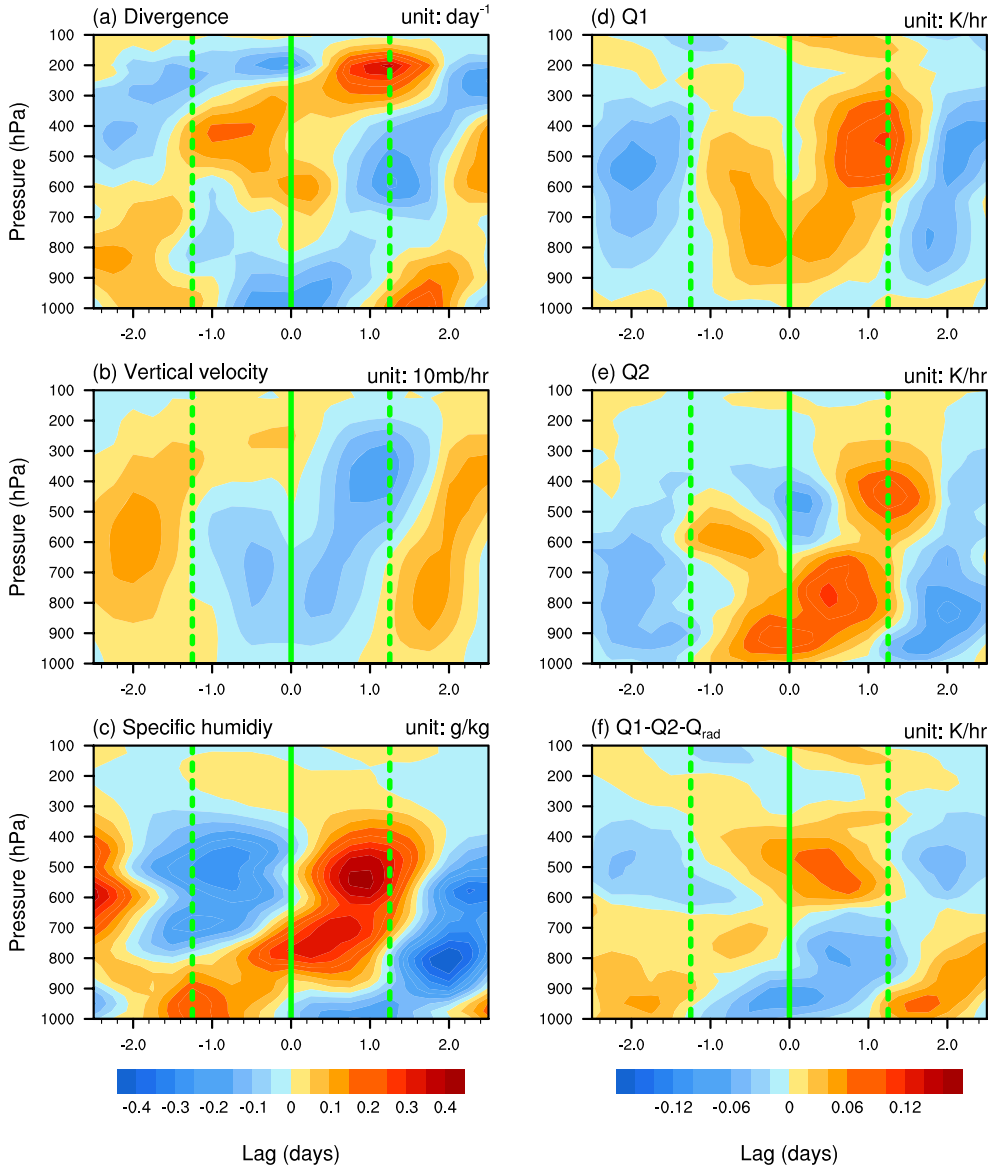

Figure 4. Composite of anomalies of (a) horizontal wind divergence (unit: day^{-1}), (b) pressure vertical velocity (unit: 10 mb/h), (c) specific humidity (g/kg), (d) apparent heating $Q1$ (unit: K/h), (e) $Q2$, (unit: K/h), and (f) $Q1 - Q2 - Q_{rad}$ (unit: K/h).

In the later phase of low-level convergence, surface humidity decreases (Figure 4c) and surface temperature becomes lower (Figure 3c). The top heavy $Q1$ and $Q2$ together with small values of $Q_1 - Q_2 - Q_{rad}$ are consistent with diabatic heating from stratiform precipitation. The stratiform-like heating has been pointed as important in producing instability for wave-convection coupling [e.g., *Mapes*, 2000; *Lin et al.*, 2004; *Kuang*, 2008].

Once the surface humidity becomes lower and surface temperature becomes cold, convection ceases. Large-scale subsidence follows to warm and dry the troposphere. This is then followed by a gradual buildup of surface moisture in the PBL.

4. Synthesis

Based on results presented above, we can divide the convectively coupled MRG wave into four phases as shown in Figure 5. The first phase starts with maximum low-level northerly flow and large-scale subsidence. Near-surface moisture increases as a result of PBL turbulence; tropospheric temperature increases as a result

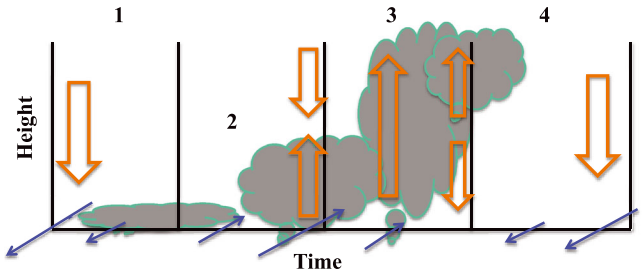

Figure 5. Schematics of four phases of the convectively coupling of MRG wave dynamics with diabatic heating. Blue arrows denote lower tropospheric meridional winds; orange broad arrows denote vertical motion; and shaded areas denote diabatic heating.

of large-scale subsidence. This phase resembles the dry MRG wave except for the moistening of the PBL. The low-level northerly decelerates the zonal wind; while the low-level easterly accelerates the meridional wind.

In the second phase, low-level southerly develops. Associated with it is low-level convergence. A key feature of this phase is that the low-level convergence is accompanied by midtropospheric divergence and upper level convergence. In this phase, lower tropospheric moisture gradually builds up which is initially caused by subgrid-scale vertical transport due to PBL turbulence and later by nonprecipitating shallow convection.

In the third phase, the diabatic heating is initially from condensational heating of shallow convection and later from deep convection with maximum heating in the upper troposphere. Deep convection causes drying and cooling near the surface.

In the fourth phase, the heating profile is initially stratiform like, with heating in the upper troposphere and cooling in the lower troposphere. The temperature and moisture near the surface become cold and dry; convection ceases to exist, which is followed by clear-sky radiative cooling and large-scale subsidence.

Similar evolution pattern of such four phases, which resembles a cumulonimbus cloud life cycle, was observed in other large-scale disturbances [e.g., *Takayabu et al.,* 1996; *Kikuchi and Takayabu*, 2004; *Mapes et al.,* 2006]. *Khouider and Majda* [2008] and *Kuang* [2008] have used similar distribution of diabatic heating to reproduce many aspects of the convectively coupled waves. The present study offers observational support to these studies with more details of the heating distribution.

5. Summary

By using the variationally analyzed winds, temperature, humidity, and diabatic heating fields from the TRMM-KWAJEX field campaign, we identified significant MRG wave activities. The wave period is found to be about 5 days. Composite analysis is presented to describe the wave structure and its coupling with the diabatic heating fields.

In the lower troposphere, the phase relationship among the meridional and zonal winds, temperature, and vertical velocity is all like the canonical MRG waves. The low-level upward vertical velocity is associated with diabatic heating that reduces the effective static stability of the wave. In the upper troposphere, however, the vertical velocity field is different from the canonical MRG waves. Maximum low-level horizontal wind convergence is accompanied by midtroposphere divergence and upper tropospheric convergence that is preceded by increase of humidity in the boundary layer. It corresponds to the successive moistening of the low troposphere and midtroposphere by PBL turbulence and shallow convection. Deep convection occurs after the low and middle troposphere becomes sufficiently moist. Deep convection produces a maximum heating center in the upper troposphere. A stratiform-like heating follows the deep convection, which is then followed by cold and dry source air and the demise of convection. Accumulation of moisture near the surface then ensues from PBL turbulence to prepare for the next phase of the convectively coupled wave.

The unique data in this study can be used to verify existing theories of convectively coupled waves, e.g., the fundamental mechanisms of the convective-dynamical instability and the front-to-rear wave tilting structure. Our analysis does not support the wave-conditional instability of the second kind hypothesis since the low-level convergence does not correspond to maximum heating. Instead, the study tends to support the

stratiform instability mechanism [e.g., *Mapes*, 2000; *Lin et al.*, 2004; *Khouider and Majda*, 2008; *Kuang*, 2008], in which the diabatic heating of the second baroclinic mode is essential in exciting the convective instability. Our study offers additional information on how the heating field is coupled with the wave in all its phases. Results can be also used to test physical parameterizations of boundary layer turbulence, shallow and deep convections in climate models.

Acknowledgments

All analyzed data in this study are available at http://atmgcm.msrc.sunysb.edu/iops.html. We thank the two anonymous reviewers whose comments have helped to improve the original paper. We wish to thank Courtney Schumacher of the Texas A& M University and Paul Ciesielski of the Colorado State University for their heroic efforts in collecting and processing the KWAJEX data that enabled the variational analysis of the diabatic heating fields used in this paper. The stimulating discussions with them have greatly benefited this work. We also thank many people and institutions who contributed to the gathering and processing of the KWAJEX, especially Sandra Yuter for her version of quality-controlled KWAJEX sounding data. This research is supported by the Major National Basic Research Program of China (973 Program) on Global Change under grant 2010CB951800, by the Biological and Environmental Research Division in the Office of Sciences of the U.S. Department of Energy (DOE), and by the National Science Foundation to the Stony Brook University. Additional support is provided by the National Natural Science Foundation of China under grant 41305102.

The Editor thanks Xiping Zeng and an anonymous reviewer for their assistance in evaluating this paper.

References

Aiyyer, A. R., and J. Molinari (2003), Evolution of mixed Rossby-gravity waves in idealized MJO environments, *J. Atmos. Sci.*, *60*, 2837–2855, doi:10.1175/1520-0469(2003)060<2837:EOMRWI>2.0.CO;2.

Blossey, P., C. Bretherton, J. Cetrone, and M. Kharoutdinov (2007), Cloud-resolving model simulations of KWAJEX: Model sensitivities and comparisons with satellite and radar observations, *J. Atmos. Sci.*, *64*, 1488–1508, doi:10.1175/JAS3982.1.

Khairoutdinov, M., and D. Randall (2003), Cloud resolving modeling of the ARM summer 1997 IOP: Model formulation, results, uncertainties, and sensitivities, *J. Atmos. Sci.*, *60*, 607–625, doi:10.1175/1520-0469(2003)060<0607:CRMOTA>2.0.CO;2.

Khouider, B., and A. Majda (2008), Equatorial convectively coupled waves in a simple multicloud model, *J. Atmos. Sci.*, *65*, 3376–3397, doi:10.1175/2008JAS2752.1.

Kikuchi, K., and Y. N. Takayabu (2004), The development of organized convection associated with the MJO during TOGA COARE IOP: Trimodal characteristics, *Geophys. Res. Lett.*, *31*, 1–4, doi:10.1029/2004GL019601.

Kistler, R., et al. (2001), The NCEP-NCAR 50-year reanalysis: Monthly means CD-ROM and documentation, *Bull. Am. Meteorol. Soc.*, *82*, 247–268, doi:10.1175/1520-0477(2001)082<0247:TNNYRM>2.3.CO;2.

Kuang, Z. (2008), A moisture-stratiform instability for convectively coupled waves, *J. Atmos. Sci.*, *65*, 834–854, doi:10.1175/2007JAS2444.1.

Li, Y., E. Zipser, S. Krueger, and M. Zulauf (2008), Cloud-resolving modeling of deep convection during KWAJEX. Part I: Comparison to TRMM satellite and ground-based radar observations, *Mon. Weather Rev.*, *136*, 2699–2712, doi:10.1175/2007MWR2258.1.

Liebmann, B., and H. Hendon (1990), Synoptic-scale disturbances near the equator, *J. Atmos. Sci.*, *47*, 1463–1479, doi:10.1175/1520-0469(1990)047<1463:SSDNTE>2.0.CO;2.

Lin, J., B. Mapes, M. Zhang, and M. Newman (2004), Stratiform precipitation, vertical heating profiles, and the Madden-Julian oscillation, *J. Atmos. Sci.*, *61*, 296–309, doi:10.1175/15200469(2004)061<0296:SPVHPA>2.0.CO;2.

Lin, J. L., et al. (2006), Tropical intraseasonal variability in 14 IPCC AR4 climate models. Part I: Convective signals, *J. Clim.*, *19*(12), 2665–2690, doi:10.1175/JCLI3735.1.

Lindzen, R. S. (1974), Wave-CISK in the tropics, *J. Atmos. Sci.*, *31*, 156–179, doi:10.1175/1520-0469(1974)031<0156:WCITT>2.0.CO;2.

Mapes, B. E. (2000), Convective inhibition, subgrid-scale triggering energy, and stratiform instability in a toy tropical wave model, *J. Atmos. Sci.*, *57*, 1515–1535, doi:10.1175/1520-0469(2000)057<1515:CISSTE>2.0.CO;2.

Mapes, B. E., S. Tulich, J. Lin, and P. Zuidema (2006), The mesoscale convection life cycle: Building block or prototype for large-scale tropical waves?, *Dyn. Atmos. Oceans*, *42*, 3–29, doi:10.1016/j.dynatmoce.2006.03.003.

Neelin, J. D., and I. M. Held (1987), Modeling tropical convergence based on the moist static energy budget, *Mon. Weather Rev.*, *115*, 3–12, doi:10.1175/1520-0493(1987)115<0003:MTCBOT>2.0.CO;2.

Schumacher, C., and R. Houze (2000), Comparison of radar data from the TRMM satellite and Kwajalein oceanic validation site, *J. Appl. Meteorol.*, *39*, 2151–2164, doi:10.1175/15200450(2001)040<2151:CORDFT>2.0.CO;2.

Schumacher, C., M. Zhang, and P. Ciesielski (2007), Heating structures of the TRMM field campaigns, *J. Atmos. Sci.*, *64*, 2593–2610, doi:10.1175/JAS3938.1.

Schumacher, C., P. Ciesielski, and M. Zhang (2008), Tropical cloud heating profiles: Analysis from KWAJEX, *Mon. Weather Rev.*, *136*, 4289–4300, doi:10.1175/2008MWR2275.1.

Sobel, A., S. Yuter, C. Bretherton, and G. Kiladis (2004), Large-scale meteorology and deep convection during TRMM KWAJEX, *Mon. Weather Rev.*, *132*, 422–444, doi:10.1175/15200493(2004)132<0422:LMADCD>2.0.CO;2.

Straub, K. H., and G. N. Kiladis (2003), The observed structure of convectively coupled Kelvin waves: Comparison with simple models of coupled wave instability, *J. Atmos. Sci.*, *60*, 1655–1668, doi:10.1175/1520-0469(2003)060<1655:TOSOCC>2.0.CO;2.

Swann, A., A. Sobel, S. E. Yuter, and G. N. Kiladis (2006), Observed radar reflectivity in convectively coupled Kelvin and mixed Rossby-gravity waves, *Geophys. Res. Lett.*, *33*, 1–4, doi:10.1029/2006GL025979.

Tai, K.-S., and Y. Ogura (1987), An observational study of easterly waves over the eastern Pacific in the northern summer using FGGE data, *J. Atmos. Sci.*, *44*, 339–361, doi:10.1175/15200469(1987)044<0339:AOSOEW>2.0.CO;2.

Takayabu, Y. N., and T. Nitta (1993), 3–5 day-period disturbances coupled with convection over the tropical Pacific Ocean, *J. Meteorol. Soc. Jpn.*, *71*, 221–246.

Takayabu, Y. N., K.-M. Lau, and C.-H. Sui (1996), Observation of a quasi-2-day wave during TOGA COARE, *Mon. Weather Rev.*, *124*, 1892–1913, doi:10.1175/1520-0493(1996)124<1892:OOAQDW>2.0.CO;2.

Wang, X., and M. Zhang (2013), An analysis of parameterization interactions and sensitivity of single-column model simulations to convection schemes in CAM4 and CAM5, *J. Geophys. Res. Atmos.*, *118*, 8869–8880, doi:10.1002/jgrd.50690.

Wheeler, M., and G. N. Kiladis (1999), Convectively coupled equatorial waves: Analysis of clouds and temperature in the wavenumber-frequency domain, *J. Atmos. Sci.*, *56*, 374–399, doi:10.1175/1520-0469(1999)056<0374:CCEWAO>2.0.CO;2.

Yanai, M., S. K. Esbensen, and J. H. Chu (1973), Determination of bulk properties of tropical cloud clusters from large-scale heat and moisture budgets, *J. Atmos. Sci.*, *30*, 611–627, doi:10.1175/1520-0469(1973)030<0611:DOBPOT>2.0.CO;2.

Yokoyama, C., and Y. N. Takayabu (2012), Relationships between rain characteristics and environment. Part II: Atmospheric disturbances associated with shallow convection over the eastern tropical Pacific, *Mon. Weather Rev.*, *140*, 2841–2859, doi:10.1175/MWR-D-11-00251.1.

Yuter, S., R. Houze, E. Smith, T. Wilheit, and E. Zipser (2005), Physical characterization of tropical oceanic convection observed in KWAJEX, *J. Appl. Meteorol.*, *44*, 385–415, doi:10.1175/JAM2206.1.

Zeng, X., W.-K. Tao, S. Lang, A. Y. Hou, M. Zhang, and J. Simpson (2008), On the sensitivity of atmospheric ensembles to cloud microphysics in long-term cloud-resolving model simulations, *J. Meteorol. Soc. Jpn.*, *86*, 45–65, doi:10.2151/jmsj.86A.45.

Zhang, C. (2005), Madden-Julian oscillation, *Rev. Geophys.*, *43*, 1–36, doi:10.1029/2004RG000158.

Zhang, C., and S. Hagos (2009), Bi-modal structure and variability of large-scale diabatic heating in the tropics, *J. Atmos. Sci.*, *66*, 3621–3640, doi:10.1175/2009JAS3089.1.

Zhang, M., and J. Lin (1997), Constrained variational analysis of sounding data based on column-integrated budgets of mass, heat, moisture, and momentum: Approach and application to ARM measurements, *J. Atmos. Sci.*, *54*, 1503–1524, doi:10.1175/1520-0469(1997)054<1503:CVAOSD>2.0.CO;2.

Zhang, M., and M. Geller (1994), Selective excitation of tropical atmospheric waves in wave-CISK: Effect of vertical wind shear, *J. Atmos. Sci.*, *51*, 353–368, doi:10.1175/1520-0469(1994)051<0353:SEOTAW>2.0.CO;2.

Zhang, M., J. Lin, R. Cederwall, J. Yio, and S. Xie (2001), Objective analysis of ARM IOP data: Method and sensitivity, *Mon. Weather Rev.*, *129*, 295–311, doi:10.1175/1520-0493(2001)129<0295:OAOAID>2.0.CO;2.

Zhang, Y. C., W. B. Rossow, and A. A. Lacis (1995), Calculation of surface and top of atmosphere radiative fluxes from physical quantities based on ISCCP data sets: 1. Method and sensitivity, *J. Geophys. Res.*, *100*, 1149–1165, doi:10.1029/94JD02747.